NanoTBTech

Nanoparticles-based 2D thermal bioimaging technologies

H2020-FETOPEN-1-2016-2017

Grant Agreement: 801305

Deliverable number D6.1 (D6)

First Calibration Datasheets for *in vivo* Imaging

Final Version

Project Deliverable Information Sheet

NanoTBTech Project	Project Ref. No. 801305
	Project Title: *Nanoparticles-based 2D thermal bioimaging technologies*
	Project Website: http://www.nanotbtech.eu/
	Deliverable No.: D6
	Deliverable Type: Report
	Dissemination Level: Public
	Contractual Delivery Date: 31 May 2019
	Actual Delivery Date: 16 May 2019
	EC Project Officer: Barbara GERRATANA

Document Control Sheet

Document	Title: First calibration datasheets for *in vivo* imaging
	Version: Final
	Available at: Participant's Portal
Authorship	Written by: FUNDACION PARA LA INVESTIGACION BIOMEDICA DEL HOSPITAL UNIVERSITARIO RAMON Y CAJAL (FIBIRYCIS)
	Contributed by: - CENTRE NATIONAL DE LA RECHERCHE SCIENTIFIQUE CNRS (CNRS) - AGENCIA ESTATAL CONSEJO SUPERIOR DE INVESTIGACIONES CIENTIFICAS (CSIC) - BIOSPACE LAB (BL)
	Approved by: all partners

History of Changes

Version	Date	Description	Reviewer
V0	27.04.2019.	Version 0	FIBIRYCIS
V1	15.05.2019.	Version 1	Prof. Luis Carlos
V2	15.05.2019	Version 2	WP1
Final Version	16.05.2019	Final Version	All partners

*This project has received funding from the European Union's Horizon 2020 research and innovation programme under grant agreement No **801305.***

Abbreviations and Acronyms

Ag_2S	Silver sulfidez
BW	Biological window
CCD	Charged-coupled device
CNRS	Centre National de la Recherche Scientifique
CSIC	Agencia Estatal Consejo Superior de Investigaciones Cientificas
FIBIRYCIS	Fundacion para la Investigacion Biomedica del Hospital Universitario Ramon Y Cajal
InGaAs	Indium gallium arsenide
LNThs	Luminescent Nanothermometers
MPA	3-mercaptopropionic acid
MPEGA	Metoxy-Polyethylene glycol acid
NIR	Near Infra-Red
NPs	Nanoparticles
PEGA	Polyethylene glycol acid
PhenA	(1,10-phenanthrolin-4-yl)methyl acrylate
PL	Photoluminescence
QDs	Quantum dots
TEM	Transmission electron microscopy
UAVR	Universidade de Aveiro
WP	Work package(s)
WPAS	Instytut Niskich Temperatur I Badan Strukturalnych Im. Wlodzimierza Trzebiatowskiego Polskiej Akademii Nauk
XRD	X-Ray Diffraction

*This project has received funding from the European Union's Horizon 2020 research and innovation programme under grant agreement No **801305.***

Table of Contents

*This project has received funding from the European Union's Horizon 2020 research and innovation programme under grant agreement No **801305.***

D6.1 FIRST CALIBRATION DATASHEETS FOR *IN VIVO* IMAGING

Work package 6 (WP6) of the project is titled: "Real time in vivo thermal images in BW-II and BW-III for tumour detection, tumour monitoring and magnetic/optical hyperthermia". The report is mainly given by a lead beneficiary of the WP6: Fundacion para la Investigacion Biomedica del Hospital Universitario Ramon y Cajal (FIBIRYCIS); along with other partners:

- Centre National de la Recherche Scientifique (CNRS)
- Agencia Estatal Consejo Superior De Investigaciones Cientificas (CSIC)
- Biospace Lab (BL)

This report identifies the nanostructures that satisfy the minimum requirements for *in vivo* thermal imaging in BW-II and BW-III based on their specific properties (thermal sensitivity, biocompatibility, biofunctionalization, tumour targeting etc). Additionally, it provides the calibration datasheets corresponding to the nanostructures.

*This project has received funding from the European Union's Horizon 2020 research and innovation programme under grant agreement No **801305.***

1 Minimum requirements for *in vivo* thermal imaging

Up to now, the vast majority of luminescent nanothermometers (LNThs) with potential to work subcutaneously have demonstrated to be capable, at least in principle, of dynamical (time resolved) 1D (punctual) subcutaneous thermal reading.[1] However, since the main goal of this project is to achieve 2D subcutaneous thermal imaging technologies, some challenges need to be faced. Going from 1D to 2D subcutaneous thermal reading is not an easy task. Indeed other well established methods have failed in undergoing this transition. For instance, thermographic cameras have been demonstrated to be capable of accurate contactless 2D in vivo dynamic thermal imaging but only at the surface of tissues (skin) with negligible penetration capability.[2,3]

Despite the large number of nanostructures capable of behaving as LNThs, only a few of them show real potential for *in vivo* thermal imaging. This is so because most of them operate in the visible spectrum domain, where optical penetration into tissues is minimal. In order to avoid this limitation, one would have to shift their operation spectral range from the visible to one of the so-called biological windows (BWs), where both tissue absorption and scattering are minimized.[4,5] There are, traditionally, three biological optical transparency windows (BW-I: 650–950 nm, BW-II: 1000–1350 nm, BW-III: 1500–1800 nm), each of them contributing in a different manner to deep tissue imaging prospects.[6–8] In terms of imaging, the BW-I has the inconvenience of signal interference by tissue autofluorescence,[9] nevertheless its remarkable tissue penetration properties are commonly exploited for effective near infrared (NIR) laser excitation. ([9,10]) If one looks into literature, one will find out 808 nm as the optimum excitation wavelength as it minimizes both the laser-induced thermal loading of the tissue and the intracellular photochemical damage.[11–14] Additionally, the existence of high power, cost-effective laser diodes operating at 808 nm made this specific wavelength interesting from the technical point of view.[15] The BW-II is significantly better suited for NIR imaging at greater tissue depths while BW-III offers improved imaging contrast due to extremely reduced NIR light scattering.[11,16–23] Moreover, the NIR light in both the BW-II and BW-III provides high signal-to-noise ratio for in vivo imaging by effectively filtering out autofluorescence.[20,21] Thus, the eventual ambition of achieving *in vivo* thermal imaging by using LNThs would benefit from the concurrent use of all three available BWs: exciting the NPs in the BW-I (specifically at 808 nm) and collecting their emission in BW-II and/or BW-III.[24–26]

However, even if a LNTh satisfies those conditions, *in vivo* thermal imaging can still remain unachievable due to the relatively low thermal sensitivities (defined as $S_R = |d\Delta/dT|/\Delta$, where Δ is the thermometric parameter) provided by most LNThs working in the BW-II and BW-III (not much higher than 10^{-3} °C^{-1}). These low thermal sensitivities make it very difficult for the commercially available shortwave infrared cameras to acquire low-noise fluorescence images and, therefore, to reconstruct accurate bidimensional thermal images.[27,28] Thus, a good LNTh candidate for *in vivo* thermal imaging should have a relatively high thermal sensitivity. Finally, but not less important, one should also consider the chemical stability and biocompatibility of the nanostructures. After all, a bright and highly sensitive LNTh would be of no practical use in biomedicine if it was to harm the tissues under study.

*This project has received funding from the European Union's Horizon 2020 research and innovation programme under grant agreement No **801305.***

With the previous discussion in mind, one can conceive a flow diagram that needs to be followed in the selection of promising nanostructures. Figure 1 sums up the general questions one has to ask before considering a certain LNTh as candidate for *in vivo* thermal imaging. Once a LNTh passes this test, one needs to compare its brightness, thermal sensitivity and biocompatibility with other candidates that were previously selected (if there were others) in order to make a list of the most promising nanostructures.

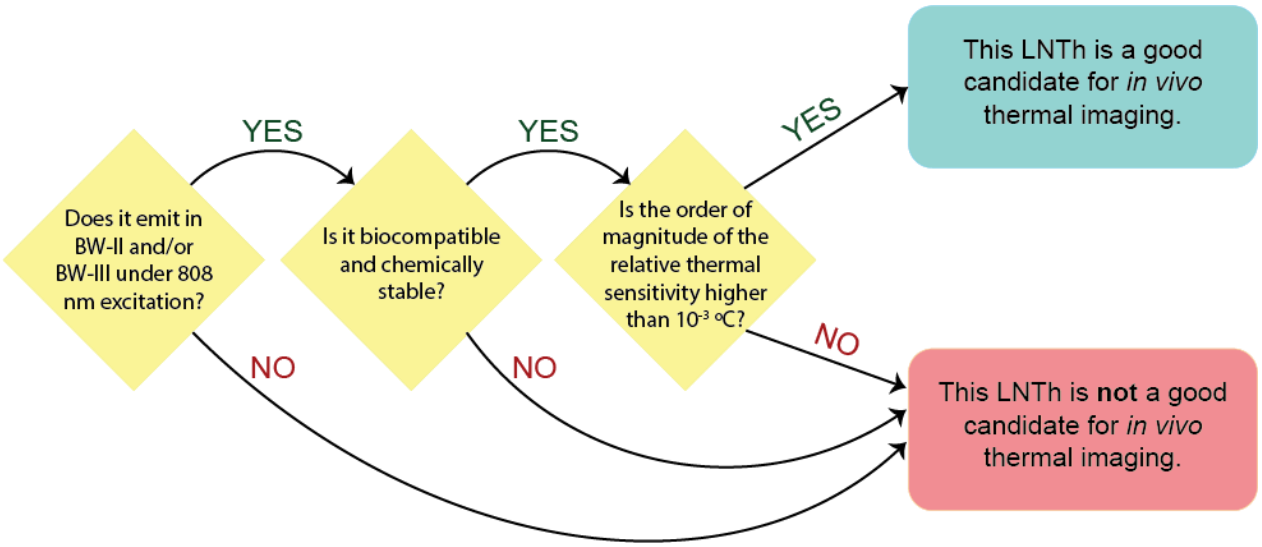

Figure 1. Flow diagram followed in the selection of the most promising nanostructures as candidates for *in vivo* thermal imaging.

*This project has received funding from the European Union's Horizon 2020 research and innovation programme under grant agreement No **801305.***

2 Characterization of the nanostructures – Experimental Conditions

If one looks back into Figure 1, it is easy to notice that a series of experiments must take place in order to answer the questions that are contained in it. The first question is answered if one looks for emission in BW-II or BW-III after exciting the NPs at 808 nm excitation. The second question is answered by studying the dependence of the emission spectra of the NPs as a function of temperature. The third question, in turns, is answered by evaluating the time evolution of biological parameters and activities of small animals after administering the NPs at a certain concentration. In the following subsections, one will find a brief description of the experimental conditions corresponding to these experiments.

2.1 Photoluminescence spectroscopy

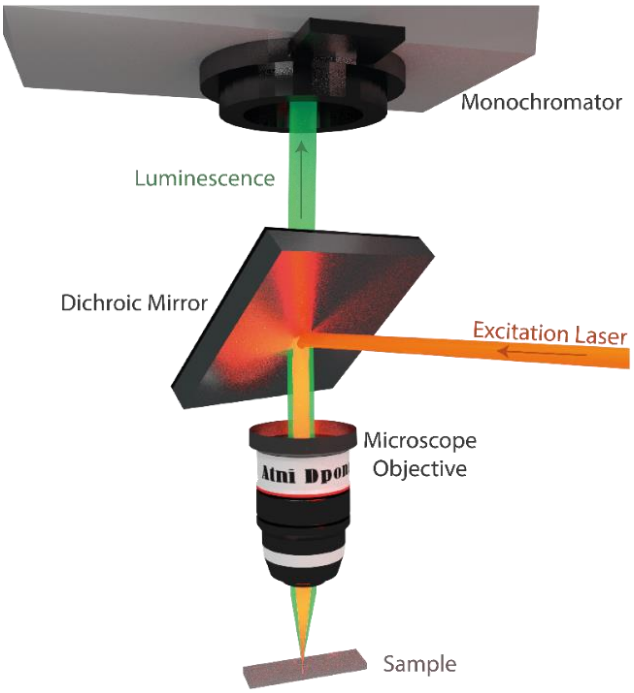

Figure 2. Schematic representation of the experimental setup used for PL spectroscopy. An 808 nm laser beam is focused into a sample and its luminescence is collected by the same focusing objective. The luminescence is spectrally analysed by a monochromator and finally collected by a CCD camera.

A microscope was used to obtain the infrared emission spectra of the nanostructures (see Figure 2). An 808 nm laser diode was coupled to a fiber and connected to a collimator (Thorlabs PAFA-X-4-B). The laser beam, after being reflected in a dichroic mirror, was focused on a microchamber with 100 µl of the nanostructures in water, by means of a microscope objective (OLYPUMS LMPlan IR 50x/0.55 ∞/0). The laser power at the focus position was established as 19.6 mW. Luminescence was collected

*This project has received funding from the European Union's Horizon 2020 research and innovation programme under grant agreement No **801305.***

by the same microscope objective and, after passing through the dichroic mirror, which filtered the radiation corresponding to the excitation laser, was spectrally analyzed by a monochromator (Andor Shamrock 193i) and finally collected by a CCD camera (InGaAs Andor iDus DU490A-1.7). The slit aperture and the integration time were fixed to 400 μm and 0.3 s, respectively. For the recording of the spectra, the Andor SOLIS software, provided by manufacturers, was utilized.

2.2 Biocompatibility

The established biocompatibility test constituted of analysing the time evolution of weight, daily food intake and temperature of a group of four CD1 mice after intravenous administration of 300 μL of a dispersion of the NPs in PBS at a concentration of 0.5 mg/mL. This, in turns, constituted a total administration dose of 150 μg (5 mg/kg). Simultaneously, a second group of four CD1 mice was used as a control group after the intravenous injection of 300 μL of PBS. The animals were housed in two separated cages in a room (23 ± 2°C) maintained on a 12/12 h light/dark cycle with free access to food and water. Weight, food intake and surface temperature, as measured by an infrared thermographic camera (FLIR E-40), were analysed in the awake mice on a daily basis for 2 weeks.

2.3 Thermal Sensing

The relative thermal sensitivity, S_R, of a thermometer is a quantity that might depend not only on the selected thermometric parameter but also on the experimental setup being used. For this reason, three subsets of experiments were conducted. The first was performed in the setup described in Section 2.1 and took as the thermometric parameter either the luminescence intensity, the intensity ratio of the emission at different wavelengths or the wavelength position of maximum intensity. The second was similar to the first but was performed on a setup that was more appropriate for two-dimensional thermal imaging. The third, finally, took the luminescence lifetime as the thermometric parameter and was performed on a setup appropriate for time resolved spectroscopy.

2.3.1 Calibration as measured with a microscope

The measurement of the calibration curves of the intensity, the intensity ratio of emission at different wavelengths or the wavelength position of the maximum was first performed using the experimental setup described in Section 2.1. The difference, of course, being the addition of a thermoelectrically Peltier plate cooled by a refrigerated circulating water bath (MX07R-20-A1 Heidolph) to the microscope stage. This system allowed the selection, with an accuracy of 0.1 ° C, of temperatures between and -25 and 120 °C. For the calibration curves, however, we only considered the physiological temperature range (10 – 50 °C).

*This project has received funding from the European Union's Horizon 2020 research and innovation programme under grant agreement No **801305.***

2.3.2 Calibration as measured with an IR imaging device

In order to test if the nanostructures were sensitive enough for *in vivo* thermal imaging, an infrared imaging system (IR-VIVO 20219 by *Photon Etc*) was used to obtain the thermal dependence of their spectral hypercube, *i.e.* a set of luminescence images corresponding to wavelengths found in the 900-1600 nm range. This system was composed of a filter wheel for multispectral filtering, a HyperCube™ for hyperspectral filtering and an InGaAs camera (ZephIR 1.7™) for detection (see Figure 3). The samples, in contact with a thermoelectrically Peltier plate (SEGA INVEX 2018-0110), were put on a supporting platform at a suitable distance from the InGaAs camera and illuminated by a fiber-coupled diode laser operating at 808 nm (whose distance to the sample was set to 16 cm). The illumination power density was set to 24 mW. The luminescence was then collected and spectrally analyzed by the HyperCube™ (spectral resolution: 6 nm) before getting to the InGaAs camera. The integration time was fixed to 1 s. For the recording of the luminescence images and spectra, the PHySpec™ software, provided by manufacturers, was utilized.

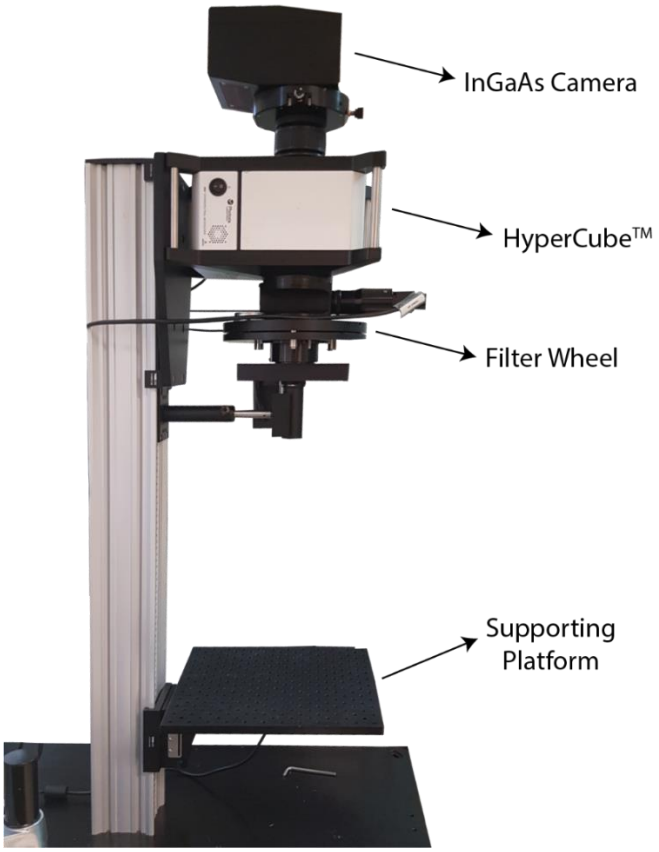

Figure 3. Representative picture of the infrared imaging system used for calibrations measurements and, potentially, *in vivo* thermal imaging in near future.

*This project has received funding from the European Union's Horizon 2020 research and innovation programme under grant agreement No **801305.***

2.3.3 Calibration as measured with time resolved spectroscopy

Luminescence decay curves were obtained by exciting the colloidal suspensions of Ag2S NCs by a OPO oscillator pumped by frequently doubled Nd:YAG laser (Lotis), which provides 8 ns pulses at a repetition rate of 10 Hz. The pulse energy was 0.1 mJ. The fluorescence intensity was detected with a Peltier cooled photomultiplier tube with enhanced sensitivity in the NIR-II (Hamamatsu R5509-73). Its voltage was set to -500 mV. The contribution of scattered laser radiation was removed by using two bandpass filters (Thorlabs FEL850) and a high brightness monochromator (Andor Shamrock 320). The time evolution of the fluorescence signal was recorded and averaged by a digital oscilloscope (Le Croy Waverunner 6000).

3 Calibration datasheets of the chosen nanostructures

After following the flow diagram of Figure 1 and considering the results obtained with the experiments of Section 2, the nanostructures known as PEGylated Ag2S superdots (provided by Grupo De Investigación Materiales Nanoestructurados Bioactivos at Universiad Complutense de Madrid, directed by Prof. Jorge Rubio Retama) have presented themselves as the best possible candidates so far. In a brief description, these nanostructures are derived from chemically synthesized Ag_2S quantum dots, on which a protective shell is grown by femtosecond laser irradiation. This shell, in turns, reduces the structural defects and minimizes the probability of non-radiative deexcitation, increasing their fluorescence lifetime from 200 ns up to 2 μs. Simultaneously, an 80-fold enhancement of the quantum yield (from 0.13% to 10.7 %) is also achieved. As a consequence, PEGylated Ag2S superdots enable deep-tissue *in vivo* imaging at low excitation power densities (<1 mW/cm2) and minimum administration doses (<0.5 mg/kg). The combination of all these properties, in turns, makes them unrivalled contrast agents for at least NIR-II bioimaging. Furthermore, the low toxicity of Ag_2S quantum dots together with the ability of AgCl coatings to minimize a NP cytotoxicity, makes them very suitable in terms of biocompatibility.[29,30]

Finally, but in no such way less important, these nanostructures also present a relatively high thermal sensitivity. Thus, they are not only biocompatible contrast agents for NIR-II bioimaging but also very good thermometers. For this reason, the datasheets and graphs describing their calibration curves (as mentioned in Section 2.2) are included in the following subsections.

3.1 Calibration Curve – Microscope

The calibration measurements performed on the microscope are summarized in Figure 4. Figure 4a depicts the emission spectra obtained at different temperatures. Figure 4a, b and c, in turns, depict the calibration curves obtained for the following thermometric parameters: integrated emission intensity (Int_{Em}), wavelength position of the maximum (λ_{Imax}) and ratio between the emission intensities at 1249 nm and 1168 nm (I_{1249nm}/I_{1168nm}). Their datasheets are included in **Table 1**. As one can see from the figures and Table 1, the calibrations were performed twice. In the first time, the

*This project has received funding from the European Union's Horizon 2020 research and innovation programme under grant agreement No **801305.***

temperature T was increased from 21 to 46 ºC. In the second, it was decreased from 46 to 21 ºC. Since this was the first calibration experiment to be conducted, this cyclical variation of temperature had to be performed in order to demonstrate the absence of a hysteresis problem, i.e. when a thermometer appears to have a memory effect when moved through a sequential range of temperatures. According to what is seen in Figure 4, the results suggest no evidence for that effect in Ag_2S superdots, especially when considering the error bars associated to the intrinsic uncertainty of the measurement and the equipment utilized.

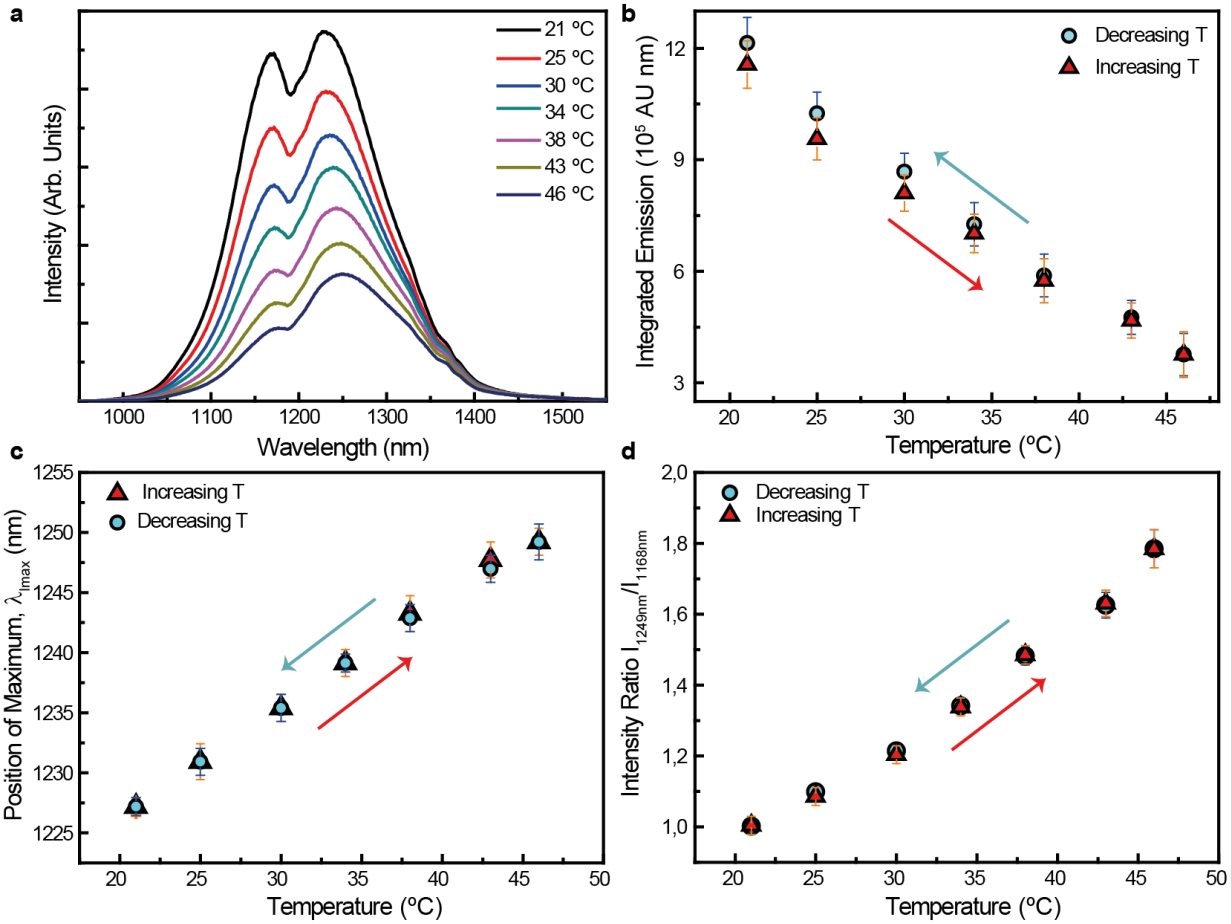

Figure 4. (a) Luminescence spectra of Ag_2S superdots as obtained with the microscope setup (section 2.2.1) at different temperatures. Calibration curves of (b) integrated emission intensity, (c) wavelength position of the maximum and (d) ratio between the emission intensities at 1249 nm and 1168 nm.

*This project has received funding from the European Union's Horizon 2020 research and innovation programme under grant agreement No **801305.***

If one fits the data contained in Table 1 to linear functions, one will find the values for the linear and angular coefficients to be equal to the ones inserted in **Table 2**. With these values one can uniquely convert a measurement of Int_{Em}, λ_{Imax} or I_{1249nm}/I_{1168nm} into temperature units. Additionally, one can estimate the relative thermal sensitivities at 21 ^{o}C as 2.59, 0.07 and 3.09 % $^{o}C^{-1}$ for Int_{Em}, λ_{Imax} and I_{1249nm}/I_{1168nm}, respectively. This, in turns, suggests that λ_{Imax} is not a good parameter to be used in thermal imaging, especially considering the spectral resolution of a common IR imaging device (Section 2.2.2) where a variation λ_{Imax}.

Temperature (°C)	(↑ ***T***)			(↓ ***T***)		
	Int_{Em} (10^6Counts · nm)	λ_{Imax} (nm)	I_{1249nm}/I_{1168nm} (dimensionless)	Int_{Em} (10^6Counts · nm)	λ_{Imax} (nm)	I_{1249nm}/I_{1168nm} (dimensionless)
21	1.15595	1227.18	1.0046	1.21412	1227.18	1.0021
25	0.95644	1230.92	1.0859	1.02464	1230.92	1.0988
30	0.81018	1235.40	1.2036	0.86792	1235.40	1.2144
34	0.70182	1239.14	1.3385	0.72631	1239.14	1.3412
38	0.57459	1243.25	1.4854	0.58869	1242.87	1.4818
43	0.46746	1247.73	1.6307	0.47598	1246.98	1.6256
46	0.37592	1249.22	1.7845	0.37590	1249.22	1.7844

Table 1. Calibration datasheets of different thermometric parameters when increasing (↑ ***T***) or decreasing temperature (↓ ***T***).

Thermometric Parameter	**Linear Fit:** $A + B \times T$			
	A	**ΔA**	**B**	**ΔB**
Int_{Em}	1.7316×10^6 (Counts · nm)	0.0516×10^6 (Counts · nm)	-2.9868×10^4 (Counts·nm·^{o} C^{-1})	0.1478×10^4 (Counts·nm·^{o} C^{-1})
λ_{Imax}	1208.32095 (nm)	0.72259 (nm)	0.90548 (nm·^{o} C^{-1})	0.0207 (nm·^{o} C^{-1})
I_{1249nm}/I_{1168nm}	0.31005 (dimensionless)	0.05522 (dimensionless)	0.03107 ($°C^{-1}$)	0.00158 ($°C^{-1}$)

Table 2. Linear and angular coefficients obtained when fitting the data contained in Figure 4b, c and d to a linear function. ΔA and ΔB stand for the errors in the calculation of the linear and angular coefficients, respectively.

3.2 Calibration Curve – IR Imaging Device

The calibration measurements performed on the IR imaging device are summarized in Figure 5. Figure 5a depicts the emission spectra obtained at different temperatures. Correspondingly, Figure 5b contains the luminescence images corresponding to the 1230 nm emission of the solutions inserted in the microchamber for characterization as obtained at different temperatures. Similar to

*This project has received funding from the European Union's Horizon 2020 research and innovation programme under grant agreement No **801305.***

Section 3.1, Figure 5c, d and e depict the calibration curves obtained for the following thermometric parameters: integrated emission intensity (Int_{Em}), wavelength position of the maximum (λ_{Imax}) and ratio between the emission intensities at 1249 nm and 1168 nm (I_{1249nm}/I_{1168nm}). Their datasheets are included in **Table 3**. Since the hysteresis hypothesis was already disconfirmed, the calibration measurements were performed only once with no significant loss.

If one fits the data contained in **Table 3** to linear functions, one will find the values for the linear and angular coefficients to be equal to the ones inserted in **Table 4**. With these values one can uniquely convert a measurement (performed on the IR imaging device) of Int_{Em}, λ_{Imax} or I_{1249nm}/I_{1168nm} into temperature units. Additionally, one can estimate the relative thermal sensitivities at 20 ^{o}C as 3.04, 0.05 and 1.58 % $^{o}C^{-1}$ for Int_{Em}, λ_{Imax} and I_{1249nm}/I_{1168nm}, respectively. Confirming, therefore, the discussion, contained in the previous section, concerning the unsuitable use of λ_{Imax} for thermal imaging.

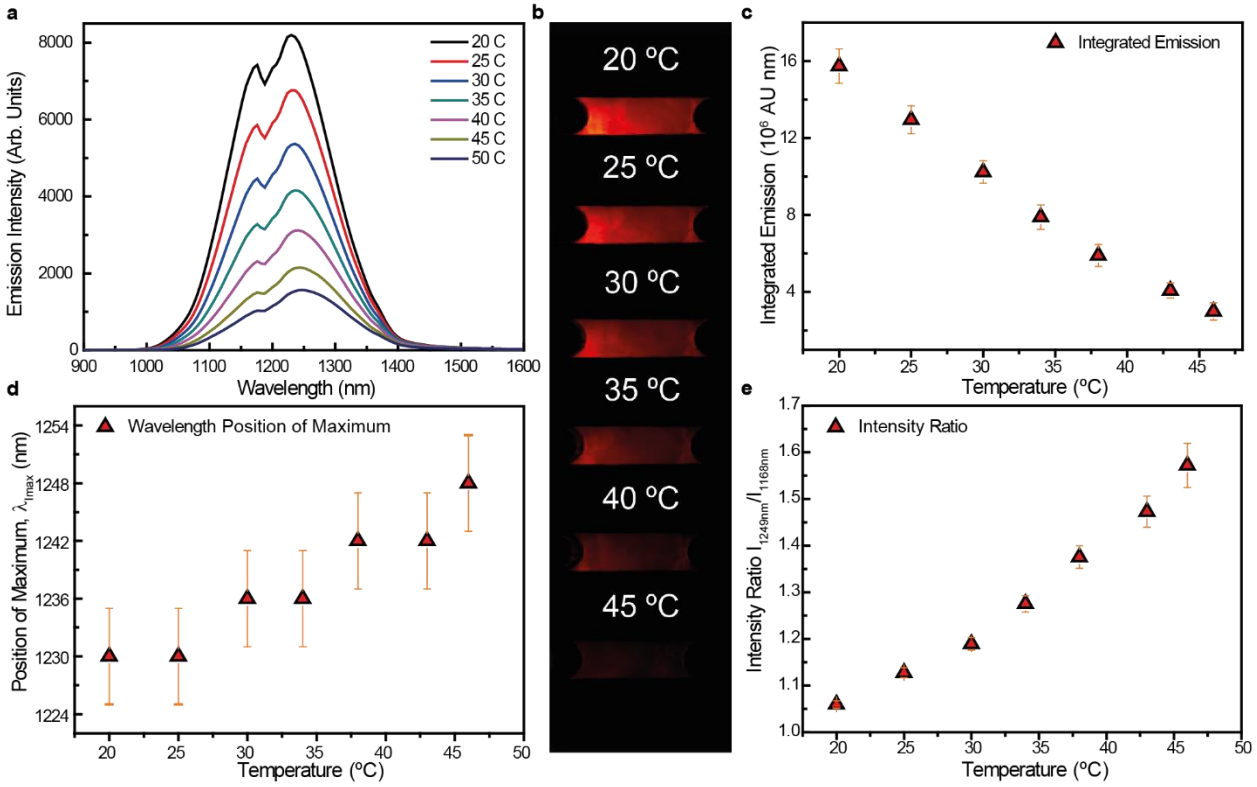

Figure 5. (a) Luminescence spectra of Ag_2S superdots as obtained with the IR imaging device (section 2.2.2) at different temperatures. (b) Images corresponding to the 1230 nm luminescence of the Ag_2S superdots solution contained in the microchamber as obtained at different temperatures. Calibration curves of (c) integrated emission intensity, (d) wavelength position of the maximum and (e) ratio between the emission intensities at 1249 nm and 1168 nm.

*This project has received funding from the European Union's Horizon 2020 research and innovation programme under grant agreement No **801305.***

Temperature (°C)	(↑ T)		
	Int_{Em} (10^6Counts · nm)	λ_{Imax} (nm)	I_{1249nm}/I_{1168nm} (dimensionless)
20	1.57382	1230	1.05972
25	1.29485	1230	1.12743
30	1.02338	1236	1.18926
34	0.78896	1236	1.27522
38	0.58989	1242	1.37549
43	0.40773	1242	1.47275
46	0.29896	1248	1.57202

Table 3. Calibration datasheets of different thermometric parameters when increasing (↑ T) or decreasing temperature (↓ T).

Thermometric Parameter	Linear Fit: $A + B \times T$			
	A	**ΔA**	**B**	**ΔB**
Int_{Em}	2.4678×10^6 (Counts · nm)	0.0768×10^6 (Counts · nm)	-4.7930×10^4 (Counts·nm·^{o} C^{-1})	0.1998×10^4 (Counts·nm·^{o} C^{-1})
λ_{Imax}	1214.74451 (nm)	3.00232 (nm)	0.68131 (nm·^{o} C^{-1})	0.0862 (nm·^{o} C^{-1})
I_{1249nm}/I_{1168nm}	0.71335 (dimensionless)	0.03321 (dimensionless)	0.01683 ($°C^{-1}$)	0.00125 ($°C^{-1}$)

Table 4. Linear and angular coefficients obtained when fitting the data contained in Figure 5b, c and d to a linear function. ΔA and ΔB stand for the errors in the calculation of the linear and angular coefficients, respectively.

3.3 Calibration Curve – Time Resolved Spectroscopy

The calibration measurements performed on the time resolved spectroscopy equipment are summarized in Figure 6. Figure 6a depicts the luminescence decay curves obtained at different temperatures. Similar to the previous sections, Figure 6b depicts the calibration curves obtained for the luminescence lifetime of the nanostructure (τ) as obtained under 808 nm excitation. The corresponding datasheet is included in **Table 5**.

If one fits the data contained in **Table 5** to a linear function, one will find the values for the linear and angular coefficients to be equal to the ones inserted in **Table 6**. With these values one can uniquely convert a measurement of τ into temperature units. Additionally, one can estimate the relative thermal sensitivities at 20 ^oC as 1.65 % $^oC^{-1}$.

*This project has received funding from the European Union's Horizon 2020 research and innovation programme under grant agreement No **801305.***

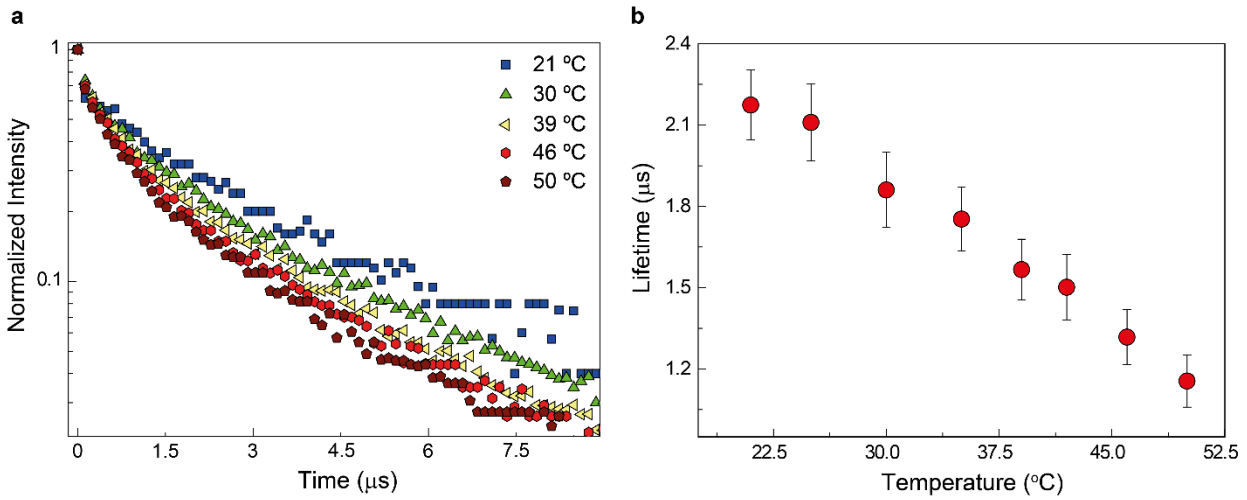

Figure 6. (a) Luminescence decay curves as obtained with the Ag_2S superdots solutions in time resolved spectroscopy (section 2.2.3) at different temperatures. Calibration curve of luminescence lifetime estimated from the decay curves.

Temperature (°C)	**(↑ *T*)**
	τ (μs)
21	2.17399
25	2.1096
30	1.86058
35	1.75268
39	1.5667
42	1.50128
46	1.31734
50	1.15538

Table 5. Calibration datasheets of different thermometric parameters when increasing (↑ ***T***) or decreasing temperature (↓ ***T***).

Thermometric Parameter	**Linear Fit: $A + B \times T$**			
	A	**ΔA**	**B**	**ΔB**
τ	2.96552 (μs)	0.0488 (μs)	-0.03576 ($\mu s \cdot {}^{o}C^{-1}$)	0.00124 ($\mu s \cdot {}^{o}C^{-1}$)

Table 6. Linear and angular coefficients obtained when fitting the data contained in Figure 6b to a linear function. ΔA and ΔB stand for the errors in the calculation of the linear and angular coefficients, respectively.

*This project has received funding from the European Union's Horizon 2020 research and innovation programme under grant agreement No **801305.***

4 General conclusions and perspectives

From the previous sections, one can conclude that the advantages offered by the Ag_2S superdots, such as good photochemical stability, optimum spectral operation range, 80-fold improvement in quantum yield and high thermal sensitivity, constitute a large step towards their translation into *in vivo* experiments. Thus, having acknowledged their evident potential, the next natural step is to measure other calibration curves under different environments that can, at least in principle, simulate their interaction with living biological tissues. This, in turns, will be main goal of the experiments that will follow this report. Once this step is finished, the direct demonstration of their thermal imaging application in small living animals can be achieved much easier.

*This project has received funding from the European Union's Horizon 2020 research and innovation programme under grant agreement No **801305.***

5 References

1. del Rosal, B., Ximendes, E., Rocha, U. & Jaque, D. In Vivo Luminescence Nanothermometry: from Materials to Applications. *Advanced Optical Materials* **5**, 1600508 (2017).
2. Godoy, S. E. *et al.* Dynamic infrared imaging for skin cancer screening. *Infrared Physics & Technology* **70**, 147–152 (2015).
3. Herman, C. The role of dynamic infrared imaging in melanoma diagnosis. *Expert Review of Dermatology* **8**, 177–184 (2013).
4. Smith, A. M., Mancini, M. C. & Nie, S. Second window for in vivo imaging. *Nature Nanotech* **4**, 710–711 (2009).
5. Anderson, R. R. & Parrish, J. A. The Optics of Human Skin. *Journal of Investigative Dermatology* **77**, 13–19 (1981).
6. Xu, J., Murata, D., Ueda, J. & Tanabe, S. Near-infrared long persistent luminescence of Er^{3+} in garnet for the third bio-imaging window. *J. Mater. Chem. C* **4**, 11096–11103 (2016).
7. Hemmer, E. *et al.* Upconverting and NIR emitting rare earth based nanostructures for NIR-bioimaging. *Nanoscale* **5**, 11339 (2013).
8. Smith, A. M., Mancini, M. C. & Nie, S. Second window for in vivo imaging. *Nature Nanotech* **4**, 710–711 (2009).
9. del Rosal, B., Villa, I., Jaque, D. & Sanz-Rodríguez, F. In vivo autofluorescence in the biological windows: the role of pigmentation. *J. Biophoton* **9**, 1059–1067 (2016).
10. De Grand, A. M. *et al.* Tissue-like phantoms for near-infrared fluorescence imaging system assessment and the training of surgeons. *J. Biomed. Opt.* **11**, 014007 (2006).
11. Zhang, Y. *et al.* Ag2S Quantum Dot: A Bright and Biocompatible Fluorescent Nanoprobe in the Second Near-Infrared Window. *ACS Nano* **6**, 3695–3702 (2012).
12. Nyk, M., Kumar, R., Ohulchanskyy, T. Y., Bergey, E. J. & Prasad, P. N. High Contrast in Vitro and in Vivo Photoluminescence Bioimaging Using Near Infrared to Near Infrared Up-Conversion in Tm^{3+} and Yb^{3+} Doped Fluoride Nanophosphors. *Nano Lett.* **8**, 3834–3838 (2008).
13. Li, X. *et al.* Nd3+ Sensitized Up/Down Converting Dual-Mode Nanomaterials for Efficient In-vitro and In-vivo Bioimaging Excited at 800 nm. *Sci Rep* **3**, 3536 (2013).
14. Hong, G. *et al.* In Vivo Fluorescence Imaging with Ag_2S Quantum Dots in the Second Near-Infrared Region. *Angew. Chem. Int. Ed.* **51**, 9818–9821 (2012).
15. Zhan, Q. *et al.* Using 915 nm Laser Excited Tm3+/Er 3+/Ho3+-Doped NaYbF4 Upconversion Nanoparticles for in Vitroand Deeper in Vivo Bioimaging without Overheating Irradiation. *ACS Nano* **5**, 3744–3757 (2011).
16. Robinson, J. T. *et al.* In Vivo Fluorescence Imaging in the Second Near-Infrared Window with Long Circulating Carbon Nanotubes Capable of Ultrahigh Tumor Uptake. *J. Am. Chem. Soc.* **134**, 10664–10669 (2012).
17. Hong, G. *et al.* Multifunctional in vivo vascular imaging using near-infrared II fluorescence. *Nat Med* **18**, 1841–1846 (2012).
18. Hong, G. *et al.* In Vivo Fluorescence Imaging with Ag_2S Quantum Dots in the Second Near-Infrared Region. *Angew. Chem.* **124**, 9956–9959 (2012).

*This project has received funding from the European Union's Horizon 2020 research and innovation programme under grant agreement No **801305.***

19. Tao, Z. *et al.* Biological Imaging Using Nanoparticles of Small Organic Molecules with Fluorescence Emission at Wavelengths Longer than 1000 nm. *Angew. Chem. Int. Ed.* **52**, 13002–13006 (2013).
20. Villa, I. *et al.* 1.3 μm emitting SrF2:Nd3+ nanoparticles for high contrast in vivo imaging in the second biological window. *Nano Res.* **8**, 649–665 (2015).
21. Diao, S. *et al.* Biological imaging without autofluorescence in the second near-infrared region. *Nano Res.* **8**, 3027–3034 (2015).
22. Naczynski, D. J. *et al.* Rare-earth-doped biological composites as in vivo shortwave infrared reporters. *Nat Commun* **4**, 2199 (2013).
23. Wang, R., Li, X., Zhou, L. & Zhang, F. Epitaxial Seeded Growth of Rare-Earth Nanocrystals with Efficient 800 nm Near-Infrared to 1525 nm Short-Wavelength Infrared Downconversion Photoluminescence for In Vivo Bioimaging. *Angew. Chem. Int. Ed.* **53**, 12086–12090 (2014).
24. Sordillo, L. A., Pu, Y., Pratavieira, S., Budansky, Y. & Alfano, R. R. Deep optical imaging of tissue using the second and third near-infrared spectral windows. *J. Biomed. Opt* **19**, 056004 (2014).
25. Skripka, A. *et al.* Double rare-earth nanothermometer in aqueous media: opening the third optical transparency window to temperature sensing. *Nanoscale* **9**, 3079–3085 (2017).
26. Hemmer, E., Benayas, A., Légaré, F. & Vetrone, F. Exploiting the biological windows: current perspectives on fluorescent bioprobes emitting above 1000 nm. *Nanoscale Horiz.* **1**, 168–184 (2016).
27. Brites, C. D. S. *et al.* Thermometry at the nanoscale. *Nanoscale* **4**, 4799 (2012).
28. Ximendes, E. C. *et al.* In Vivo Subcutaneous Thermal Video Recording by Supersensitive Infrared Nanothermometers. *Adv. Funct. Mater.* **27**, 1702249 (2017).
29. Zhang, Y. *et al.* Biodistribution, pharmacokinetics and toxicology of Ag2S near-infrared quantum dots in mice. *Biomaterials* **34**, 3639–3646 (2013).
30. Lu, C., Chen, G., Yu, B. & Cong, H. Recent Advances of Low Biological Toxicity Ag2S QDs for Biomedical Application. *Adv. Eng. Mater.* **20**, 1700940 (2018).

*This project has received funding from the European Union's Horizon 2020 research and innovation programme under grant agreement No **801305.***